SECED 2023 Conference
Earthquake Engineering & Dynamics for a Sustainable Future
14-15 September 2023, Cambridge, UK

SEISMIC RESPONSE PREDICTION FOR NON-STRUCTURAL COMPONENTS IN MULTI-STOREY STRUCTURES

X. Ding[1], M. Liapopoulou[2] & A.Y. Elghazouli[3]

Abstract *This paper investigates the seismic response of non-structural components and proposes analytical expressions to estimate their spectral accelerations, with the aim of improving European code provisions. A series of non-structural components with varying periods and strength reduction factors are modelled as single-degree-of-freedom systems that are fixed on each floor of 38 primary structures. The primary structures are steel moment-resisting frames of three, five, and seven storeys, designed to Eurocode 8. Nonlinear time history analyses are carried out, using 100 far-field and near-field ground motion records, scaled at two intensity levels to represent elastic and inelastic primary structures. Based on the results, regression analyses are performed to derive predictive equations for the spectral acceleration of non-structural components, considering their first two modes of vibration. The proposed equations are compared to those in the upcoming Eurocode 8 revision and to the analysis results. It is shown that the revised Eurocode 8 offers relatively accurate predictions that closely fit the analytical accelerations near the fundamental period, but significant deviations are observed further away, especially for inelastic primary structures. The proposed modified equations are shown to improve the overall accuracy and overcome the shortcomings of code provisions, particularly those related to the inadequate consideration of the inelasticity of non-structural components.*

Keywords*: non-structural components, seismic response, Eurocode 8*

Introduction

Compared with structural components, non-structural components (NSCs) are typically more vulnerable to earthquake damage. For example, common damage types observed in NSCs during the 1994 Northridge, the 2011 Christchurch, and the 2016 Central Italy earthquakes included extensive cracks in partition masonry walls, overturning of medical equipment, and torsional failure of water pipes (Baird et al., 2014); (Charleson, 2012). Although most buildings remained structurally undamaged during these events, many lost their function because of the failure of NSCs. In addition, the monetary investment in NSCs is considerable, usually reaching up to 80% of the total investment (Shahram Taghavi, 2006). Therefore, in order to ensure the full operation of buildings and a low maintenance cost, it is necessary to provide a reliable estimate of the expected behaviour of non-structural components at the initial stages of design.

The validity of the current EC8 procedures for non-structural components has been the subject of various recent investigations, with the aim of developing more accurate evaluation and prediction procedures (Kazantzi, Vamvatsikos & Miranda, 2020; Lucchini, Franchin & Mollaioli, 2017; Vukobratović & Fajfar, 2015). After a series of systematic efforts, Vukobratovic & Fajfar (2015) proposed a detailed prediction framework, which was implemented in the proposed second generation EC8 revision (*CEN/TC 250/SC 8 N 941.*).

In this paper, the accuracy of the current and revised EC8 provisions is investigated. For this purpose, NSCs with varying periods and strength reduction factors are considered on each floor of 38 primary steel moment-resisting frames. The systems are subjected to nonlinear time history analyses, using 100 far-field and near-field ground motion records, scaled at two intensity levels to represent elastic and inelastic primary structures. Comparative assessments are then carried out, and modifications are proposed to improve the accuracy of the revised EC8 provisions.

[1] PhD student, Imperial College London, London, United Kingdom, xiapeng.ding18@imperial.ac.uk
[2] Postdoctoral researcher, Imperial College London, London, United Kingdom
[3] Professor, Imperial College London, London, United Kingdom

Methodology

Structural configurations

The numerical models for the primary structures and the non-structural components were constructed in OpenSees (McKenna, 2011). The primary structures are 3-, 5-, and 7-storey steel moment frames, designed to EC3 and EC8 provisions for various combinations of Ground Types and drift limits. They are regular in plan and elevation, as shown in Figure 1. Hence, the ground motion input for the primary structures and the floor acceleration input for the NSCs can be simplified by considering only one horizontal component.

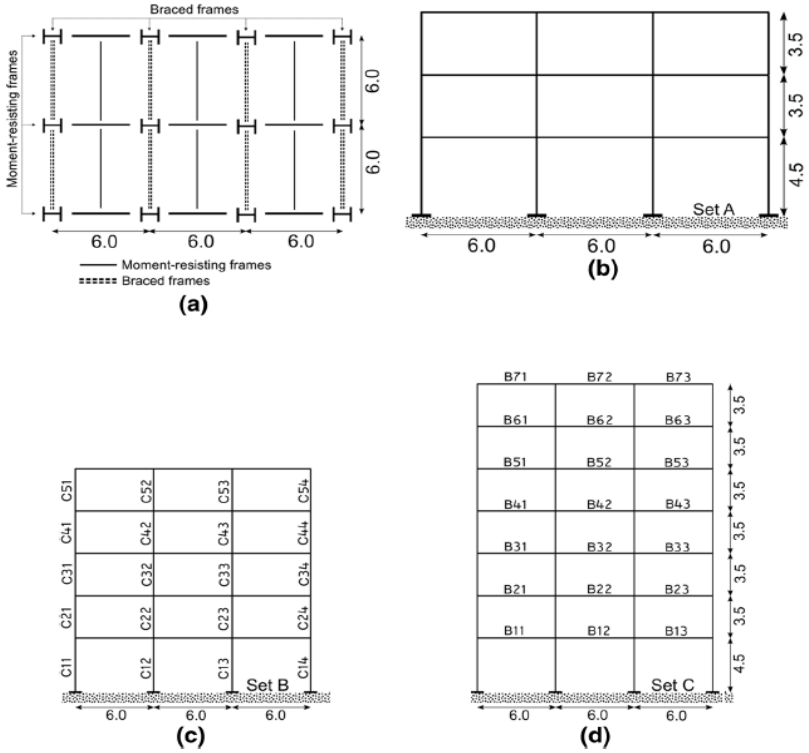

Figure 1. Primary structures and typical elevations: (a) plan, (b) 3-storey frames, (c) 5-storey frames, and (d) 7-storey frames (Bravo-Haro & Elghazouli, 2018).

The primary structures were modelled using the lumped plasticity approach. Accordingly, rotational springs were attached at the ends of columns and beams, representing plastic hinges. Their hysteretic behaviour was defined based on the Ibarra-Medina-Krawinkler hysteretic model (Ibarra, Medina & Krawinkler, 2005; Lignos & Krawinkler, 2011), considering strength and stiffness degradation. The panel zones were modelled as a rectangular assembly of rigid, pin-connected elements. The shear-distortion behaviour of panel zones was represented through a zero-length spring at the top right corner, whose characteristics were defined by a trilinear hysteretic model (Gupta, 1999). More detailed information on the design, modelling, and structural characteristics of the frames can be found elsewhere (Bravo-Haro & Elghazouli, 2018).

Both elastic and inelastic material behaviour was considered for the primary structures. However, only a limited degree of inelasticity was assumed herein, as investigation of the NSCs response is only meaningful if the primary structure exhibits small plastic deformation levels. Hence, two levels were considered for the behaviour factor of primary structures; $R_{ps} = 1$, which corresponded to an elastic primary structure, and $R_{ps} = 2$, which corresponded to an inelastic primary structure.

For the NSCs, uncoupled analysis, also referred to as Floor Response Spectra Method (FRS method), can be adopted. Based on the ASCE 4-16 (2017) criteria, if the mass of the secondary system is significantly smaller than the mass of the primary system, then coupling between the two is not required. The weight of the NSCs examined herein is considerably smaller than that of the floor where they are mounted, and hence, they are decoupled from the primary structure.

The NSCs are modelled as a lumped mass fixed at the free end of a vertical cantilever, which is fixed on each floor level, and they are subjected to the predetermined input floor response acceleration history. Apart from the floor excitation, their seismic response is otherwise only related to their inherent structural characteristics. Their period of vibration T_{an} is varied from 0.05s to 4.0s, with a 0.05s step. Elastic NSCs, as well as inelastic NSCs with 5 levels of lateral strength demand are considered. Hence, the behaviour factor of NSCs is varied within the range of $R_{nsc} = 1, 2, 3, 4, 5, \text{and } 6$.

Ground motion records

In order to cover as many different ground motion characteristics as possible, two different types of ground motion records are considered herein, namely far-field records and near-field records. In total, 100 ground motion acceleration records are assembled (44 far-field records and 56 near-field records) from 50 realistic seismic events. The near field records can be further classified into 28 records with velocity pulses and 28 records without velocity pulses.

In Figure 2, the acceleration response spectra of all individual ground motion records of each group are plotted, along with the corresponding mean response spectra. As the figure shows, the near-field records have richer frequency content than their far-field counterparts, and they also exhibit more significant variations in lower natural periods.

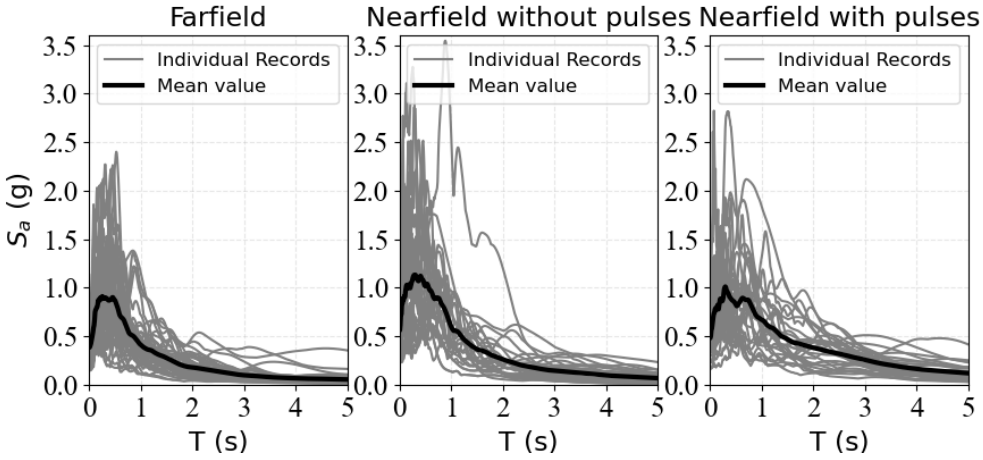

Figure 2. Unscaled spectral acceleration for each group of ground motion records.

It should be noted that the response spectra presented in Figures 2 are unscaled. To show the influence of inelastic behaviour of primary structures, the selected ground motion records should firstly be scaled before being used in subsequent Incremental Dynamic Analysis (Vamvatsikos & Cornell, 2002), as indicated in Equation (1).

$$SF = R_{str} \frac{V_1}{S_a(T_1) m \gamma_1} \tag{1}$$

Where R_{str} is the behaviour factor of the primary structure, V_1 is the base shear corresponding to the formation of the first plastic hinge in the primary structure, m is the total mass of the primary structure, and γ_1 is the effective mass participation ratio corresponding to the first vibration mode of the primary structure.

Assessment provisions

Current design guidelines include simplified procedures for assessing the seismic response of non-structural components. In this section, the current EC8 (2004) and upcoming EC8 (CEN/TC 250/SC 8, 2021) provisions are described briefly.

The current EC8 (2004) proposes Equation (2) to determine the input seismic acceleration (S_a) for non-structural components:

$$\mathrm{S_a} = \alpha S \frac{3\left[1+\frac{z}{h}\right]}{\left(1+\left[1-\frac{T_c}{T_1}\right]^2\right)} - 0.5 \leq \frac{a_g}{g} S \tag{2}$$

Where α is the ratio of the design peak ground acceleration on Type A ground to the gravitational acceleration ($\frac{a_g}{g}$), S is the soil factor in EC8 (2004) Table 3.2, T_c and T_1 are the fundamental period

of the NSC and primary structure, respectively, z is the height of NSC above the ground motion application point, and h is the total building height above the ground motion application point.

Several limitations can be observed in the above formula. The first limitation is the oversimplified linear distribution assumption. The term $\frac{z}{H}$ in Equation (2) assumes that the seismic acceleration of the NSC at each floor is a simple linear distribution along the structure height. This linear relationship was shown to result in significant inaccuracies (Aldeka, Chan & Dirar, 2014a; Aldeka, Chan & Dirar, 2014b; Aldeka et al., 2015). Secondly, the formula only accounts for the fundamental mode of primary structures, and ignores higher mode effects (Bravo-Haro & Elghazouli, 2020). Finally, the potential inelasticity of primary structures is disregarded in Equation (2).

To overcome these limitations, Vukobratovic and Fajfar (2016) proposed a direct method to determine the input floor acceleration for non-structural components. This method has been adapted in the EC8 revision (CEN/TC 250/SC 8, 2019) as follows:

$$S_{an,ij} = \frac{\Gamma_i \phi_{ij}}{\left|(\frac{T_{p,i}}{T_{an}})^2 - 1\right|} \sqrt{S_{ean}^2 + [(\frac{T_{p,i}}{T_{an}})^2 \frac{S_{ep,i}}{q_D}]^2} \tag{3}$$

$$\left|\mathrm{S_{an,ij}}\right| \leq \mathrm{AMP_i} \cdot \left|\mathrm{PFA_{ij}}\right| \tag{4}$$

$$PFA_{ij} \leq \Gamma_i \phi_{ij} \frac{S_{ep,i}}{q_D} \tag{5}$$

$$\mathrm{AMP_i} = \begin{cases} 2.5\sqrt{\frac{10}{5+\xi_{\mathrm{p,i}}}}, \frac{\mathrm{T_{p,i}}}{\mathrm{T_c}} = 0 \\ \text{linear between } \mathrm{AMP_i}\left(\frac{\mathrm{T_{p,i}}}{\mathrm{T_c}} = 0\right) \text{ and } \mathrm{AMP_i}\left(\frac{\mathrm{T_{p,i}}}{\mathrm{T_c}} = 0.2\right), 0 \leq \frac{\mathrm{T_{p,i}}}{\mathrm{T_c}} \leq 2 \\ \frac{10}{\sqrt{\xi_{\mathrm{p,i}}}}, \frac{\mathrm{T_{p,i}}}{\mathrm{T_c}} \geq 0.2 \end{cases} \tag{6}$$

Where $S_{ep,i}$ is the acceleration coordinate for the corresponding natural periods of primary structures from the input elastic design spectra, while S_{ean} is that of the NSCs from the same input elastic design spectra. $S_{an,ij}$ is the floor acceleration at the j^{th} floor for the i^{th} vibration mode. $T_{p,i}$ and T_{an} are the natural period of the i^{th} vibration mode for primary structures and NSCs, respectively. q_D is the structural behaviour factor of primary structures. T_C is the characteristic periods of the input elastic design spectrum of ground motions, which is equal to 1.0s. Φ_{ij} is the i^{th} mode shape value at j^{th} floor for primary structures, and Γ_i is the modal participation factor of i^{th} vibration mode for primary structures. $\xi_{p,i}$ and ξ_{an} are the viscous damping ratios of the primary structure and NSC, respectively.

Based on multi-degree of freedom representations (Yasui et al., 1993), Vukobratovic and Fajfar (2016) suggested an improved approach. As Equation (3) shows, the introduction of modal analysis not only considers the influence of higher vibration modes of primary structures, but also simulates the seismic response at each floor more realistically, as opposed to the oversimplified linear distribution assumption adopted in the current EC8 (2004). Subsequently, in the revised EC8 draft (CEN/TC 250/SC 8, 2021), Equation (4) is replaced with Equation (7), as follows:

$$\left|\mathrm{S_{an,ij}}\right| \leq 7 \cdot \left|\mathrm{PFA_{ij}}\right| \tag{7}$$

Comparative evaluations

In this section, the results from the OpenSees simulations are compared with predictions obtained from the current and revised EC8 provisions. Among the 38 primary frames, Frame C13, which has a fundamental period of $T_1 = 1.108s$, is selected as a representative structure herein. The mean spectral accelerations of elastic NSCs attached to the top floor of Frame C13 is plotted in Figures 3. The results are presented both for elastic and inelastic primary structures, and for each record set. In addition, the predicted spectral accelerations, based on the current and revised EC8, are plotted in each figure panel.

As shown in Figure 3, the current EC8 (2004) significantly overestimates the seismic demands at the fundamental period of the primary structure and also provide higher estimates for the seismic response of NSCs with longer periods. It is also clear that the current provisions cannot capture the change in seismic performance due to the inelastic behaviour of the primary structure.

Furthermore, a key issue in the current EC8 is that it cannot reflect the resonance effect around higher natural periods of the primary structure. The last two shortcomings are overcome in the revised EC8 provisions (CEN/TC 250/SC 8, 2021). However, the first drawback still exists. For components attached to either the elastic or inelastic primary structure, the seismic acceleration is overestimated around the fundamental period of the primary structure. At higher periods, the prediction accuracy varies, depending on the inelastic behaviour of the primary structure. Similar results can also be observed for the rest of the frames. Therefore, it is necessary to propose a modification for the revised EC8 working, especially for the spectral acceleration around the first three natural periods.

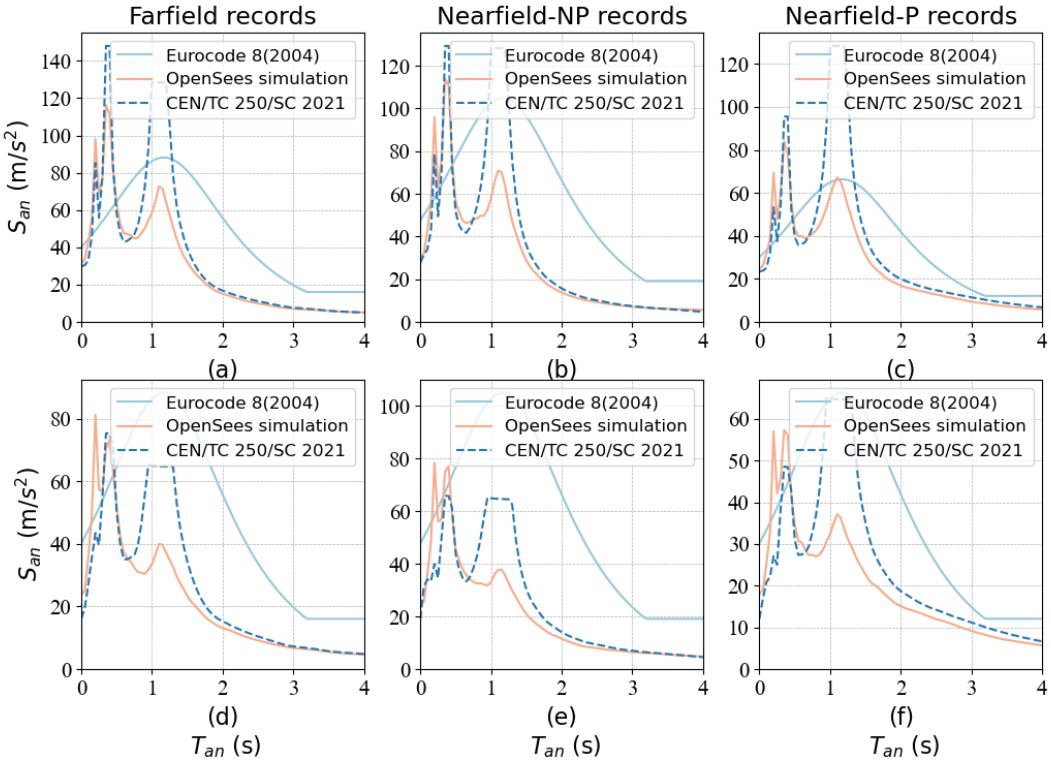

Figure 3. Spectral accelerations of elastic ($R_{nsc} = 1$) non-structural components mounted on elastic ($R_{ps} = 1$) and inelastic ($R_{ps} = 2$) Frame C13 at roof level.

Proposed modifications

Elastic components and primary structures

The case of elastic ($R_{nsc} = 1$) non-structural components mounted on elastic ($R_{ps} = 1$) primary structures is considered first. The seismic response at the roof level is considered critical, and hence, focus is given here to this aspect. A new parameter denoted 'amplification factor' (AF) is used here to demonstrate the relationship between the OpenSees results and code predictions over the whole component periods range from 0.0s to 4.0s, as shown in Equation (8).

$$AF = \frac{S_{an,op}(T_{an})}{S_{an,code}(T_{an})} \tag{8}$$

Where $S_{an,op}(T_{an})$ is the spectral acceleration from numerical results at T_{an} component period, while $S_{an,code(T_{an})}$ is the spectral acceleration from code prediction at the same component period.

In Figure 4(a), the amplification factors are plotted against the component period, normalised by the fundamental period of the primary structure, for each individual frame. The mean, mean-plus-one standard deviation, and mean-minus-one standard deviation lines are also plotted in the same figure. Based on these results, a regression equation is proposed to simulate the scatter points, as shown in Equation (9). The regression coefficients are given in Table 1.

$$AF = \frac{a_1\left(\frac{T_{an}}{T_1}\right)+c}{a_2\left(\frac{T_{an}}{T_1}\right)^4+a_3\left(\frac{T_{an}}{T_1}\right)^2+b} + d \quad (9)$$

The regression curve and the scatter points are plotted in Figure 4(b), while in Figure 4(c), the 95% confidence interval and the 95% prediction bands are also shown. The coefficient of determination $R^2 = 0.922$ is close enough to 1.0, showing that the data fit well the regression model. Also, the regression curve is well covered by the 95% confidence interval curves, indicating the high reliability of the regression analysis.

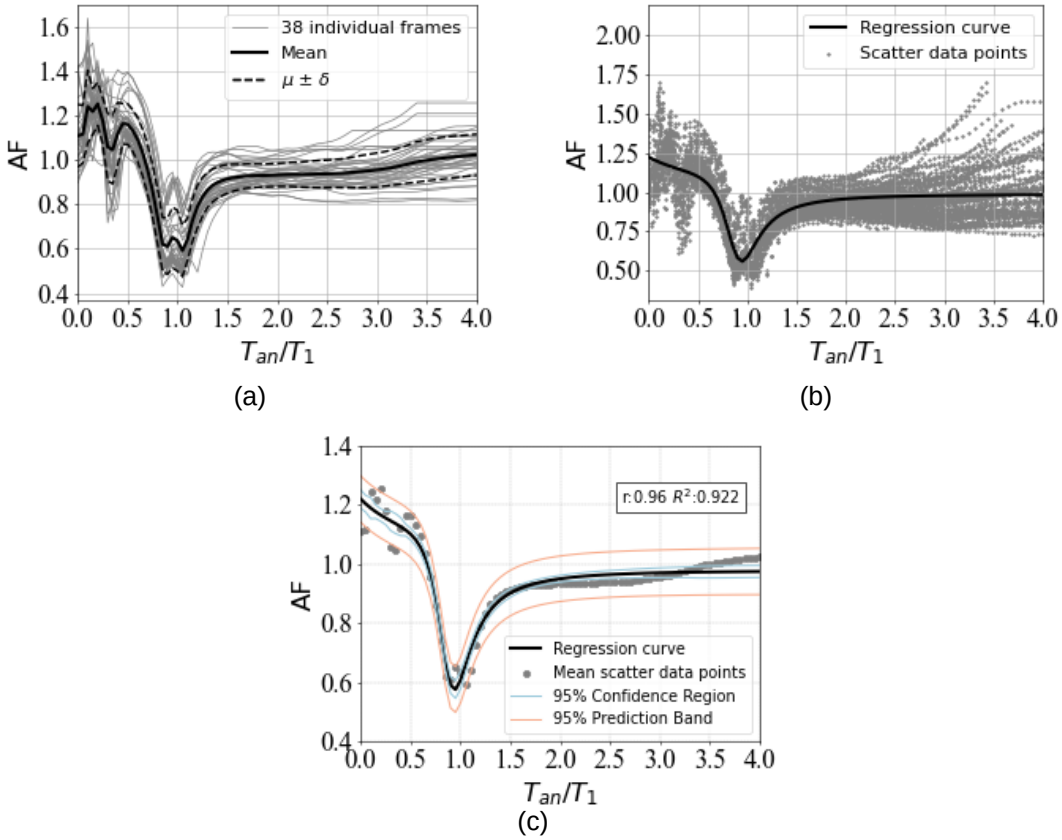

Figure 4. Amplification factors: (a) mean and one standard deviation, (b) regression curve and scatter points and (c) regression curve with prediction bands and confidence interval.

a_1	a_2	a_3	b	c	d
-1560	6834	-9952	4434	1072	1

Table 1. Regression coefficients of Equation (9).

Inelastic primary structures

Similar analyses are performed to account for the inelasticity of the primary structures. For this purpose, a new amplification factor AF_{Rstr} is defined as the ratio of the AF of the inelastic primary structure $AF_{in,p}$ over that of the elastic primary structure $AF_{e,p}$, as shown in Equation (10).

$$AF_{Rstr} = \frac{AF_{in,p}}{AF_{e,p}} \quad (10)$$

In Figure 5, AF_{Rstr} is plotted against the normalized component period for each frame, along with the mean and mean ± one standard deviation lines. The normalization is based on the fundamental period of the primary structure in Figure 5, while the second-mode period is employed in Figure 5. A distinct peak is observed around the second natural period instead of the first. Therefore, $\frac{T_{an}}{T_2}$ is used herein as the independent variable, and the regression equation is shown in Equation (11). The regression coefficients are given in Table 2.

$$AF_{Rstr} = \frac{a_1(\frac{T_{an}}{T_2})^2 + a_3(\frac{T_{an}}{T_2}) + c}{a_2(\frac{T_{an}}{T_2})^4 + b} + d \quad (11)$$

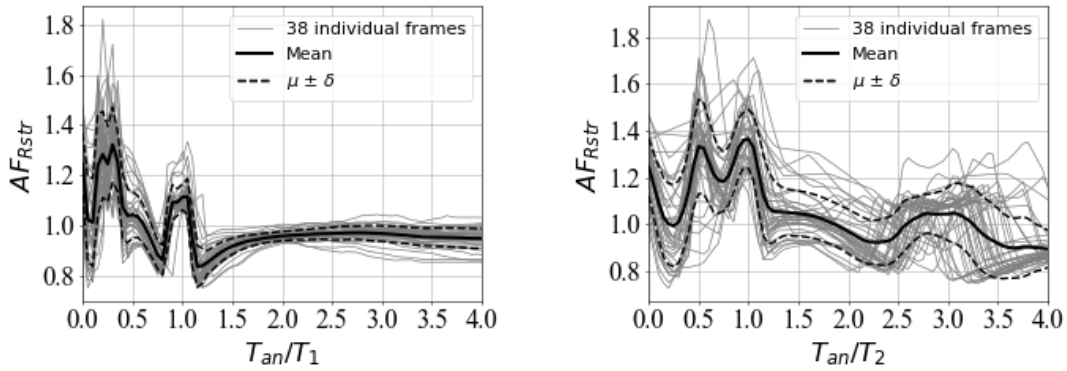

(a) (b)

Figure 5. AF_{Rstr} versus: (a) T_{an} normalised by T_1; (b) T_{an} normalised by T_2.

a_1	a_1	a_1	b	c	d
791	1664	-328	129	46	0.9

Table 2. Coefficients of Equation (11).

The regression curve along with the scatter points is plotted in Figure 6, while the 95% prediction bands and 95% confidence interval are plotted in Figure 6. The coefficient of determination $R^2 = 0.78$ is not very close to 1.0 due to the tuned effect around the second and third natural periods. A higher degree polynomial regression model could be tested to increase the coefficient of determination of the model. Nevertheless, the coefficient of determination here is still relatively large, showing that the data fit well the regression model. Also, the regression curve and data points are well covered by the 95% confidence interval curves and the 95% prediction bands respectively, indicating the high reliability of the regression analysis.

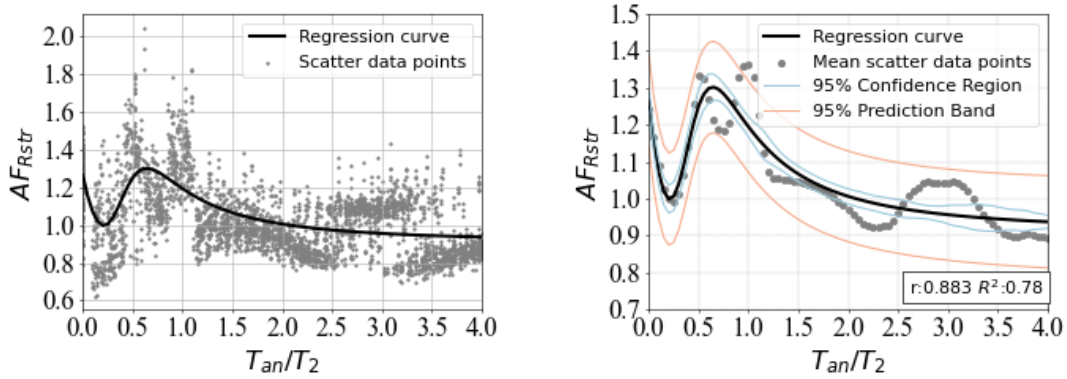

(a) (b)

Figure 6. AF_{Rstr} versus $\frac{T_{an}}{T_2}$: (a) regression curve and scatter points; (b) regression curve with prediction bands and 95% confidence interval.

Inelastic non-structural components

The final part of regression analysis is that for inelastic non-structural components on either elastic or inelastic primary structures. Similar to AF_{Rstr}, another amplification parameter AF_{Rnsc} is proposed to account for different levels of inelastic behaviour of non-structural components. This is defined as the ratio of the AF of inelastic NSCs $AF_{in,nsc}$ over that of elastic NSCs $AF_{e,nsc}$, according to Equation (12).

$$AF_{Rnsc} = \frac{AF_{in,nsc}}{AF_{e,nsc}} \tag{12}$$

In Figure 7, the amplification ratios for non-structural components at $\frac{T_{an}}{T_1} = 0.5, 1.0\ and\ 2.0$ are extracted. It is clear that the amplification factors exhibit a linear relationship against the inelastic behaviour factor of non-structural components. Furthermore, the slopes and the intercepts of the linear relationship at each specific $\frac{T_{an}}{T_1}$ are different, which has been demonstrated in Figure 7. According to this observation, the mean functional form shown in Equation (13) is selected, and the regression coefficients are listed in Table 3.

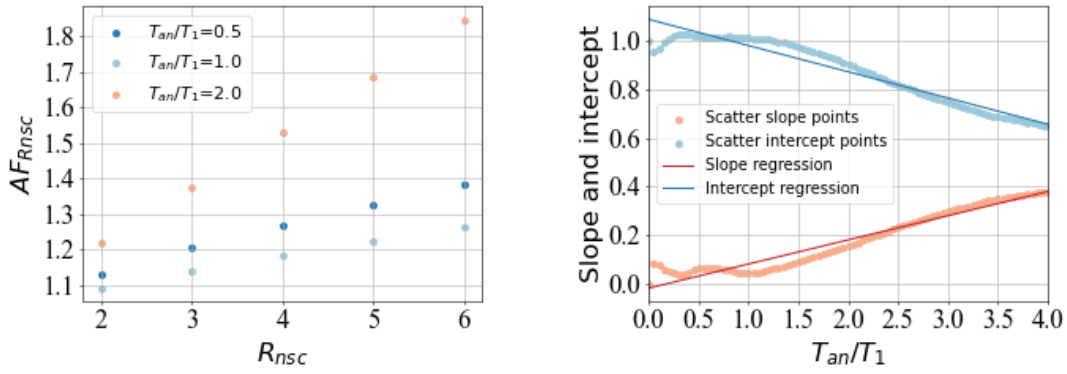

(a) (b)

Figure 7. AF_{Rnsc} for inelastic over elastic non-structural components: (a) scatter points at specific $\frac{T_{an}}{T_1}$; (b) scatter points over the whole period range along with regression curves.

$$AF_{Rnsc} = \left(a_1\left(\frac{T_{an}}{T_1}\right) + b\right) R_{nsc} + \left(a_2\left(\frac{T_{an}}{T_1}\right) + c\right) \tag{13}$$

a_1	a_2	b	c
0.1	-0.1	-0.02	1.1

Table 3. Coefficients for Equation (13).

Overall modifications

Based on the regression analyses presented above, a set of expressions in Equations (14) to (18), is proposed to update and improve the spectral acceleration predictions of NSCs in the revised EC8 provisions, as follows:

$$S_{an,p}(T_{an}) = S_{an}(T_{an}) * AF(\frac{T_{an}}{T_1}) * AF_{Rstr}(\frac{T_{an}}{T_2}) * AF_{Rnsc}(\frac{T_{an}}{T_1}) \tag{14}$$

$$AF\left(\frac{T_{an}}{T_1}\right) = \frac{-1560\left(\frac{T_{an}}{T_1}\right)+1072}{6834\left(\frac{T_{an}}{T_1}\right)^4 - 9952\left(\frac{T_{an}}{T_1}\right)^2 + 4434} + 1.0 \tag{15}$$

$$AF_{Rstr}\left(\frac{T_{an}}{T_2}\right) = \frac{791\left(\frac{T_{an}}{T_2}\right)^2 - 328\left(\frac{T_{an}}{T_2}\right)+46}{1664\left(\frac{T_{an}}{T_2}\right)^4 + 129} + 1.0 \tag{16}$$

$$AF_{Rnsc}\left(\frac{T_{an}}{T_1}\right) = \begin{cases} 1 & R_{nsc} = 1 \\ \left(0.1\left(\frac{T_{an}}{T_1}\right) - 0.02\right) R_{nsc} + \left(-0.1\left(\frac{T_{an}}{T_1}\right) + 1.0\right) & R_{nsc} \neq 1 \end{cases} \tag{17}$$

$$S_{an,p}(T_{an}) \leq S_{an,p}(T_1) \qquad 0.8T_1 \leq T_{an} \leq 1.2T_1 \tag{18}$$

Where $S_{an,p}$ is the proposed spectral acceleration of NSCs, while S_{an} is the predicted spectral acceleration of NSCs based on the revised EC8 (CEN/TC 250/SC 8, 2021). $T_{an}, T_1\ and\ T_2$ are the natural periods of NSCs, the fundamental period of primary structures, and the second natural period of primary structures, respectively.

The accuracy of the proposed modifications can be assessed by comparing the numerical results, the predictions of the revised EC8, and the modified predictions. As an example, Figure 8 plots the spectral acceleration of NSCs against their period for Frame C01 under near-field records with velocity pulses, considering varying levels of inelasticity of the primary structure and the NSC. The first-mode period of the selected frame is $T_1 = 0.89s$, while the second-mode period is $T_2 = 0.28s$. The proposed modifications are shown to rectify the overestimation of spectral accelerations around the fundamental period of the frame, as well as the underestimation around the second natural period. However, they still cannot provide a reasonable prediction for non-structural components attached on inelastic primary structures around the third or higher natural periods of the supporting frame.

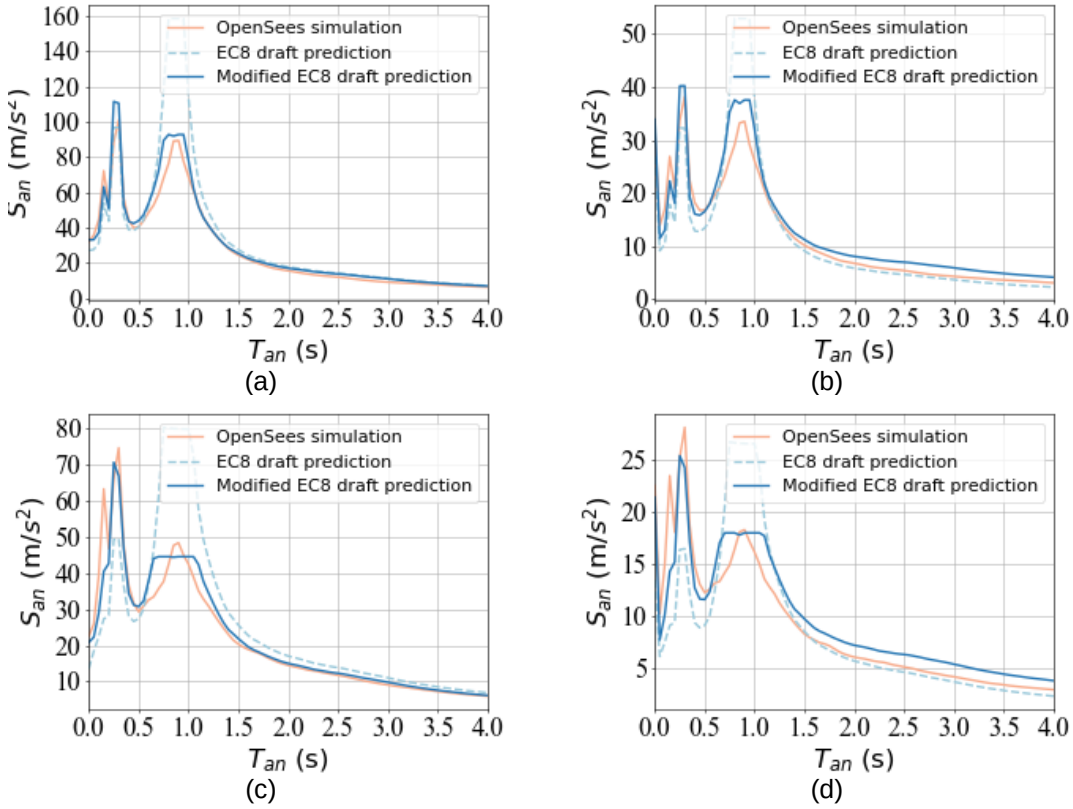

Figure 8. Spectral acceleration comparisons: (a) $R_{str} = 1$, $R_{nsc} = 1$; (b) $R_{str} = 1$, $R_{nsc} = 3$; (c) $R_{str} = 2$, $R_{nsc} = 1$; (d) $R_{str} = 2$, $R_{nsc} = 3$.

Conclusions

This paper discussed the accuracy of current and upcoming EC8 provisions for non-structural components mounted on steel multi-storey frames. The code-based spectral accelerations were compared to detailed nonlinear numerical results, based on simulations of non-structural components mounted on 38 steel moment-resisting frames. A set of 100 far-field and near-field ground motion records was employed in the analyses. It was shown that the current EC8 has several limitations, including the inability to account for inelastic primary structures and to reflect component resonance effects. In contrast, the revised EC8 procedures provide a more reliable estimation for non-structural components. However, as the component attachment height increases, the prediction accuracy deteriorates significantly. Thus, further modifications need to be proposed, with the aim to improve the accuracy of the upcoming EC8 provisions. For this purpose, three cases were considered, and regression analyses were performed to derive appropriate predictive equations: firstly, elastic non-structural components mounted on elastic primary structures; secondly, non-structural components attached to inelastic primary structures; and finally, inelastic non-structural components mounted on either elastic or inelastic primary structures. For each case, the relevant amplification factors were defined and regression analyses were performed. Combining all derived equations, a modified method was proposed to predict the spectral acceleration of non-structural components. This was compared with simulation results and estimations based on the revised EC8. Overall, although some minor shortcomings

in the case of non-structural components mounted on inelastic primary structures still exist, the proposed modification significantly improves the accuracy of the revised EC8 provisions.

References

Aldeka, A. B., Chan, A. H. C. & Dirar, S. (2014a) Response of non-structural components mounted on irregular RC buildings: comparison between FE and EC8 predictions. *Earthquakes and Structures.* 6 (4), 351-373. Available from: doi: 10.12989/eas.2014.6.4.351.

Aldeka, A. B., Chan, A. H. C. & Dirar, S. (2014b) Response of non-structural components mounted on irregular RC buildings: comparison between FE and EC8 predictions. *Earthquakes and Structures.* 6 (4), 351-373. Available from: doi: 10.12989/eas.2014.6.4.351.

Aldeka, A. B., Dirar, S., Chan, A. H. C. & Martinez-Vazquez, P. (2015) Seismic response of non-structural components attached to reinforced concrete structures with different eccentricity ratios. *Earthquakes and Structures.* 8 (5), 1069-1089. Available from: doi: 10.12989/eas.2015.8.5.1069.

Baird, A., Tasligedik, A. S., Palermo, A. & Pampanin, S. (2014) Seismic Performance of Vertical Nonstructural Components in the 22 February 2011 Christchurch Earthquake. *Earthquake Spectra.* 30 (1), 401-425. Available from: doi: 10.1193/031013EQS067M.

Bravo-Haro, M. A. & Elghazouli, A. (2020) Inelastic Displacement Ratios for Non-Structural Components in Steel Framed Structures. *September 13th to 18th 2020*.

CEN (2004). EN 1998-1: Eurocode 8: Design of structures for earthquake resistance part 1: General rules, seismic actions and rules for buildings.

CEN/TC 250/SC 8 (2019) Eurocode 8: Earthquake resistance design of structures. EN1998–1–2 working draft 19–02–2021

CEN/TC 250/SC 8 (2021) Eurocode 8: Earthquake resistance design of structures. EN1998–1–2 working draft 25–02–2021

Charleson, A. (2012) *Seismic design for architects: Outwitting the quake.* 1st edition.

Gupta, A. (1999) *Seismic demands for performance evaluation of steel moment resisting frame structures. [google]* Stanford University.

Ibarra, L. F., Medina, R. A. & Krawinkler, H. (2005) Hysteretic models that incorporate strength and stiffness deterioration. *Earthquake Engineering & Structural Dynamics.* 34 (12), 1489-1511.

Kazantzi, A. K., Vamvatsikos, D. & Miranda, E. (2020) Evaluation of seismic acceleration demands on building nonstructural elements. *Journal of Structural Engineering.* 146 (7), 04020118.

Lignos, D. G. & Krawinkler, H. (2011) Deterioration modeling of steel components in support of collapse prediction of steel moment frames under earthquake loading. *Journal of Structural Engineering.* 137 (11), 1291-1302.

Lucchini, A., Franchin, P. & Mollaioli, F. (2017) Uniform hazard floor acceleration spectra for linear structures. *Earthquake Engineering & Structural Dynamics.* 46 (7), 1121-1140.

McKenna, F. (2011) OpenSees: a framework for earthquake engineering simulation. *Computing in Science & Engineering.* 13 (4), 58-66.

Shahram Taghavi. (2006) *Seismic demand assessment on acceleration-sensitive building nonstructural components.*

Vamvatsikos, D. & Cornell, C. A. (2002) Incremental dynamic analysis. *Earthquake Engineering & Structural Dynamics.* 31 (3), 491-514.

Vukobratović, V. & Fajfar, P. (2015) A method for the direct determination of approximate floor response spectra for SDOF inelastic structures. *Bulletin of Earthquake Engineering.* 13 (5), 1405-1424. Available from: https://link.springer.com/article/10.1007/s10518-014-9667-0. Available from: doi: 10.1007/s10518-014-9667-0.

Yasui, Y., Yoshihara, J., Takeda, T. & Miyamoto, A. (1993) Direct generation method for floor response spectra.